Spectral transfers and zonal flow dynamics in the generalized Charney-Hasegawa-Mima model

C. N. Lashmore-Davies, A. Thyagaraja, and D. R. McCarthy[a]
EURATOM/UKAEA Fusion Association, Culham Science Centre, Abingdon OX14 3DB, United Kingdom

The mechanism of four nonlinearly interacting drift or Rossby waves is used as the basic process underlying the turbulent evolution of both the Charney-Hasegawa-Mima-equation (CHME) and its generalized modification (GCHME). Hasegawa and Kodama's concept of equivalent action (or quanta) is applied to the four-wave system and shown to control the distribution of energy and enstrophy between the modes. A numerical study of the GCHME is described in which the initial state contains a single finite-amplitude drift wave (the pump wave), and all the modulationally unstable modes are present at the same low level (10^{-6} times the pump amplitude). The simulation shows that at first the fastest-growing modulationally unstable modes dominate but reveals that at a later time, before pump depletion occurs, long- and short-wavelength modes, driven by pairs of fast-growing modes, grow at $2\gamma_{\max}$. The numerical simulation illustrates the development of a spectrum of turbulent modes from a finite-amplitude pump wave. © *2005 American Institute of Physics*. [DOI: 10.1063/1.2139973]

I. INTRODUCTION

In this paper a general analysis, analytical and numerical, is given of one of the simplest models of fluid/plasma turbulence. This is the Charney-Hasegawa-Mima equation (CHME) and its generalized modification, GCHME (see Refs. 1–3). These equations describe Rossby waves in atmospheric systems and electrostatic drift waves in magnetically confined plasmas. In both cases, sheared flows arise spontaneously from a background of finite-amplitude (turbulent) drift or Rossby waves. The origin of these turbulent fluctuations is not described within the CHME or GCHME. These sheared flows, referred to as zonal flows in magnetically confined plasmas are believed to be important in the evolution of transport barriers in tokamaks.[4–6] Similarly, the corresponding sheared flows, which were first noted in atmospheric systems, are believed to cause a similar reduction in transport in atmospheres.[7]

This subject was pioneered in the field of magnetically confined plasmas by Hasegawa and his co-workers[2,8,9] who took as the basic nonlinear interaction a three-wave process. By means of a heuristic analysis they observed that the system evolved to a final state containing a zonal flow (see Ref. 9). More recently, Smolyakov *et al.* (cf. Ref. 3) included the zonal flow from the outset and used a four-wave interaction as the basis for the evolution. The three-wave instability discussed by Hasegawa *et al.* was replaced by the modulational instability, and the CHME was superceded by the GCHME.

The plan of the paper is as follows. The general case of four nonlinearly interacting drift waves is discussed in Sec. II. In this paper, attention is concentrated on drift waves but the analysis and numerical simulations apply equally well to Rossby waves. Section II deals with CHME. In Sec. III, the equivalent action densities or quanta, introduced in Ref. 8 for

a three-wave interaction, are generalized to the case of a four-wave interaction. The action densities are used to demonstrate the conservation of energy and enstrophy for the four-wave interaction. The corresponding analysis for the GCHME is carried out in Sec. IV. A numerical solution of the full, nonlinear partial differential equations of the GCHME model is given in Sec. V. An interpretation of the results of the numerical simulation is given in Sec. VI and the mechanism of spectral transfer, first revealed by the simulation, is discussed. Further details of the time evolution of the modes are given in Sec. VII. The conclusions of the work are presented in Sec. VIII.

II. THE CHARNEY-HASEGAWA-MIMA EQUATION

In Refs. 8 and 9 the nonlinear coupling of three drift waves was assumed to govern the evolution of the system to a turbulent state. It was also emphasized that such an interaction could proceed not only for the resonant case, but also the nonresonant, where a significant frequency mismatch occurs. In view of this the underlying nonlinear interaction is generalized to a four-wave process. This is particularly relevant to the case where one of the interacting waves is a zero-frequency zonal flow. First, the case of four nonlinearly coupled drift waves is considered.

The starting point is the CHME,

$$\frac{\partial}{\partial t}(\nabla^2 \phi - \phi) + (\nabla \phi \times \mathbf{z}) \cdot \nabla \ln n_0 - (\nabla \phi \times \mathbf{z}) \cdot \nabla \nabla^2 \phi = 0.$$

(1)

Following Refs. 10 and 11 the time and space coordinates are normalized as follows: $\Omega_i = eB/m_i c$ is the ion cyclotron frequency in the magnetic field B (taken along the z axis), $c_s = (T_e/m_i)^{1/2}$, $\rho_s = c_s/\Omega_i$, the time is normalized to a Bohm-like diffusion time $a^2/c_s\rho_s$, and lengths to the system size a.

---

[a]Also at Southeastern Louisiana University, Hammond, LA 70402, USA.

12, 122304-1

The electrostatic potential is normalized to T_e/e. Assume the presence of four drift waves,

$$\Phi_j(\mathbf{x},t) = \phi_j(t)\exp(i\mathbf{k}_j \cdot \mathbf{x}) + \text{c.c.}, \tag{2}$$

where $j=1-4$. The wave vectors satisfy perfect wave-number matching such that

$$\mathbf{k}_3 = \mathbf{k}_1 - \mathbf{k}_2, \tag{3}$$

$$\mathbf{k}_4 = \mathbf{k}_1 + \mathbf{k}_2. \tag{4}$$

In linear theory the real frequencies of the waves are given by

$$\omega_j = -\frac{k_{jy}\alpha}{(1 + k_j^2\hat{\rho}^2)}, \tag{5}$$

where $k_j^2 = k_{jx}^2 + k_{jy}^2$, $\hat{\rho} = \rho_s/a$, and $\alpha = a/n_0(|dn_0/dx|) = a/L_n$.

The mode $(\omega_1, \mathbf{k}_1)$ will be assumed to be highly populated in comparison with the other three modes. In keeping with this assumption, the magnitudes of the wave numbers are ordered as follows:

$$k_4^2 > k_1^2 > k_3^2 > k_2^2.$$

In addition, ω_2 is taken to be the lowest frequency mode. The equations for the amplitudes $\phi_j(t)$ are obtained from Eq. (1) and are as follows:

$$\frac{d\phi_1}{dt} + i\omega_1\phi_1 = c_{23}\phi_2\phi_3 + c_{24}\phi_2^*\phi_4, \tag{6}$$

where

$$c_{23} = \frac{(k_{2x}k_{3y} - k_{2y}k_{3x})(k_3^2 - k_2^2)\hat{\rho}^2}{(1 + k_1^2\hat{\rho}^2)},$$

$$c_{24} = \frac{(k_{2y}k_{4x} - k_{2x}k_{4y})(k_4^2 - k_2^2)\hat{\rho}^2}{(1 + k_1^2\hat{\rho}^2)};$$

$$\frac{d\phi_2}{dt} + i\omega_2\phi_2 = c_{13}\phi_1\phi_3^* + c_{14}\phi_1^*\phi_4, \tag{7}$$

where

$$c_{13} = \frac{(k_{1y}k_{3x} - k_{1x}k_{3y})(k_3^2 - k_2^2)\hat{\rho}^2}{(1 + k_2^2\hat{\rho}^2)},$$

$$c_{14} = \frac{(k_{1y}k_{4x} - k_{1x}k_{4y})(k_4^2 - k_1^2)\hat{\rho}^2}{(1 + k_2^2\hat{\rho}^2)};$$

$$\frac{d\phi_3}{dt} + i\omega_3\phi_3 = c_{12}\phi_1\phi_2^*, \tag{8}$$

where

$$c_{12} = \frac{(k_{1y}k_{2x} - k_{1x}k_{2y})(k_2^2 - k_1^2)\hat{\rho}^2}{(1 + k_3^2\hat{\rho}^2)};$$

$$\frac{d\phi_4}{dt} + i\omega_4\phi_4 = d_{12}\phi_1\phi_2, \tag{9}$$

where

$$d_{12} = \frac{(k_{1x}k_{2y} - k_{1y}k_{2x})(k_2^2 - k_1^2)\hat{\rho}^2}{(1 + k_4^2\hat{\rho}^2)}.$$

Introducing the amplitudes $A_j(t)$ such that

$$\Phi_j(\mathbf{x},t) = A_j(t)\exp(-i\omega_j t)\exp(i\mathbf{k}_j \cdot \mathbf{x}) + \text{c.c.}, \tag{10}$$

and using the assumption that the mode $(\omega_1, \mathbf{k}_1)$ is highly populated compared with the other modes, the evolution of the four coupled modes can be described, initially by the equations for A_2, A_3, and A_4, which take the following forms:

$$\frac{dA_2}{dt} = c_{13}A_1A_3^*\exp(-i\delta_3 t) + c_{14}A_1^*A_4\exp(i\delta_4 t), \tag{11}$$

$$\frac{dA_3}{dt} = c_{12}A_1A_2^*\exp(-i\delta_3 t), \tag{12}$$

$$\frac{dA_4}{dt} = d_{12}A_1A_2\exp(-i\delta_4 t), \tag{13}$$

where

$$\delta_3 = \omega_1 - \omega_2 - \omega_3,$$

and

$$\delta_4 = \omega_1 + \omega_2 - \omega_4.$$

Since $A_1 \gg A_2$, A_3, and A_4, it can be assumed to remain constant during the initial stages of the evolution of Eqs. (11)–(13), thus allowing one to linearize these equations. Introducing the amplitudes,

$$\alpha_3 = \exp(-i\delta_3 t)A_3^*, \tag{14}$$

$$\alpha_4 = \exp(i\delta_4 t)A_4, \tag{15}$$

Eqs. (11)–(13) become

$$\frac{d\alpha_3}{dt} + i\delta_3\alpha_3 = c_{12}A_1^*A_2, \tag{16}$$

$$\frac{d\alpha_4}{dt} - i\delta_4\alpha_3 = d_{12}A_1A_2, \tag{17}$$

$$\frac{dA_2}{dt} = c_{13}A_1\alpha_3 + c_{14}A_1^*\alpha_4. \tag{18}$$

The set of Eqs. (16)–(18) can now be solved by assuming that A_2, α_3, and α_4 vary with time like $\exp(-i\Omega t)$ giving

$$\Omega^3 + (\delta_4 - \delta_3)\Omega^2 - [\delta_3\delta_4 - (c_{13}c_{12} + c_{14}d_{12})|A_1|^2]\Omega$$
$$+ (c_{13}c_{12}\delta_4 - c_{14}d_{12}\delta_3)|A_1|^2 = 0. \tag{19}$$

The general solution of Eq. (19) must be obtained numerically. However, denoting the left-hand side by $D(\Omega)$, there are several cases. In the first instance, if the quadratic, $\partial D/\partial\Omega = 0$, has two complex conjugate roots, Eq. (19) will have one real and two complex conjugate roots. Suppose next that there exist two real roots, Ω_1 and Ω_2 of $\partial D/\partial\Omega = 0$. When $D(\Omega_1)$ and $D(\Omega_2)$ have the same sign there will be one real root of Eq. (19) and a complex conjugate pair. In either case, one of the complex conjugate pair of roots must

be an unstable one. Finally, if $D(\Omega_1)D(\Omega_2) < 0$, all three roots of the disperison relation will be real and we will have stability. In the cases corresponding to instability, we write

$$\Omega = \Omega_r \pm i\Gamma. \tag{20}$$

The modes $(\omega_2, \mathbf{k}_2)$, $(\omega_3, \mathbf{k}_3)$, and $(\omega_4, \mathbf{k}_4)$ will be excited simultaneously by the pump wave $(\omega_1, \mathbf{k}_1)$ at the shifted frequencies $\omega_2 + \Omega_r$, $\omega_1 - \Omega_r$, and $\omega_1 + \Omega_r$, respectively.

III. FOUR-WAVE CONSERVATION RELATIONS

The conservation relations for the four-wave interaction described by Eqs. (6)–(9) will now be derived. This will be accomplished by generalizing the equivalent quanta introduced in Ref. 8 to the four-wave case. First, the equations for the wave intensities are obtained from Eqs. (6)–(9) giving

$$\frac{d|\phi_1|^2}{dt} = \frac{(k_3^2 - k_2^2)\hat{\rho}^2}{(1 + k_1^2\hat{\rho}^2)}(k_{2x}k_{3y} - k_{2y}k_{3x})(\phi_1^*\phi_2\phi_3 + \phi_1\phi_2^*\phi_3^*)$$
$$+ \frac{(k_4^2 - k_2^2)\hat{\rho}^2}{(1 + k_1^2\hat{\rho}^2)}(k_{2y}k_{4x} - k_{2x}k_{4y})$$
$$\times (\phi_1^*\phi_2^*\phi_4 + \phi_1\phi_2\phi_4^*), \tag{21}$$

$$\frac{d|\phi_2|^2}{dt} = -\frac{(k_1^2 - k_3^2)\hat{\rho}^2}{(1 + k_2^2\hat{\rho}^2)}(k_{1y}k_{3x} - k_{1x}k_{3y})(\phi_1^*\phi_2\phi_3$$
$$+ \phi_1\phi_2^*\phi_3^*) + \frac{(k_4^2 - k_1^2)\hat{\rho}^2}{(1 + k_2^2\hat{\rho}^2)}(k_{1y}k_{4x} - k_{1x}k_{4y})$$
$$\times (\phi_1^*\phi_2^*\phi_4 + \phi_1\phi_2\phi_4^*), \tag{22}$$

$$\frac{d|\phi_3|^2}{dt} = -\frac{(k_1^2 - k_2^2)\hat{\rho}^2}{(1 + k_3^2\hat{\rho}^2)}(k_{1y}k_{2x} - k_{2y}k_{1x})$$
$$\times (\phi_1^*\phi_2\phi_3 + \phi_1\phi_2^*\phi_3^*), \tag{23}$$

$$\frac{d|\phi_4|^2}{dt} = -\frac{(k_1^2 - k_2^2)\hat{\rho}^2}{(1 + k_4^2\hat{\rho}^2)}(k_{1x}k_{2y} - k_{1y}k_{2x})$$
$$\times (\phi_1\phi_2\phi_4^* + \phi_1^*\phi_2^*\phi_3). \tag{24}$$

Using the wave-number matching relations given in Eqs. (3) and (4) to express k_{3x}, k_{3y}, k_{4x}, and k_{4y} in terms of k_{1x}, k_{1y}, k_{2x}, and k_{2y}, the equivalent quanta N_i of the four modes are defined as follows:

$$N_1 = \frac{(1 + k_1^2\hat{\rho}^2)|\phi_1|^2}{\hat{\rho}^2(k_3^2 - k_2^2)(k_4^2 - k_2^2)\hat{\rho}^2}, \tag{25}$$

$$N_2 = \frac{(1 + k_2^2\hat{\rho}^2)|\phi_2|^2}{\hat{\rho}^2(k_1^2 - k_3^2)(k_4^2 - k_1^2)\hat{\rho}^2}, \tag{26}$$

$$N_3 = \frac{(1 + k_3^2\hat{\rho}^2)|\phi_3|^2}{\hat{\rho}^2(k_1^2 - k_2^2)(k_4^2 - k_2^2)\hat{\rho}^2}, \tag{27}$$

$$N_4 = \frac{(1 + k_4^2\hat{\rho}^2)|\phi_4|^2}{\hat{\rho}^2(k_1^2 - k_2^2)(k_3^2 - k_2^2)\hat{\rho}^2}. \tag{28}$$

Note that the equivalent quantum of a given mode depends

on the wave numbers of the *other* interacting modes. With the aid of the equivalent quanta the following two conservation relations are obtained:

$$\frac{d}{dt}(N_1 + N_3 + N_4) = 0, \tag{29}$$

$$\frac{d}{dt}\left[N_2 + \frac{(k_4^2 - k_2^2)}{(k_4^2 - k_1^2)}N_3 + \frac{(k_3^2 - k_2^2)}{(k_3^2 - k_1^2)}N_4\right] = 0. \tag{30}$$

In contrast with the three-wave interaction analyzed in Ref. 8, where three equivalent conservation relations for the three equivalent quanta were obtained, only two conservation relations are obtained for the four-wave interaction. Hence, the four-wave interaction equations are not integrable and may have chaotic solutions.

Consider incremental changes ΔN_i to the N_i quantities. Normalizing to the pump-wave increment ΔN_1, Eqs. (29) and (30) become

$$1 + \frac{\Delta N_3}{\Delta N_1} + \frac{\Delta N_4}{\Delta N_1} = 0, \tag{31}$$

$$\frac{\Delta N_2}{\Delta N_1} + \frac{(k_4^2 - k_2^2)}{(k_4^2 - k_1^2)}\frac{\Delta N_3}{\Delta N_1} + \frac{(k_3^2 - k_2^2)}{(k_3^2 - k_1^2)}\frac{\Delta N_4}{\Delta N_1} = 0. \tag{32}$$

Introducing the following notations:

$$-\frac{\Delta N_2}{\Delta N_1} = X_2, \tag{33}$$

$$-\frac{\Delta N_3}{\Delta N_1} = X_3, \tag{34}$$

$$-\frac{\Delta N_4}{\Delta N_1} = X_4, \tag{35}$$

it is worth remarking that X_2, X_3, and X_4 are all positive since initially, the pump wave decreases, $\Delta N_1 < 0$, while the other modes increase, $\Delta N_i > 0$ for $i = 2-4$. Hence, Eqs. (31) and (32) become

$$X_3 + X_4 = 1, \tag{36}$$

$$\frac{(k_4^2 - k_2^2)}{(k_1^2 - k_4^2)}X_3 + \frac{(k_3^2 - k_2^2)}{(k_1^2 - k_3^2)}X_4 = X_2. \tag{37}$$

Combining the last two equations, one obtains

$$\left[\frac{(k_3^2 - k_2^2)}{(k_1^2 - k_3^2)} + \frac{(k_4^2 - k_2^2)}{(k_4^2 - k_1^2)}\right]X_4 + \frac{(k_4^2 - k_2^2)}{(k_1^2 - k_4^2)} = X_2. \tag{38}$$

Since $0 < X_4 < 1$, Eq. (38) constrains the range of values that X_2 may take, depending on the values of the k_i^2.

The energies of the modes W_i can be obtained from the energy invariant of the CHM Eq. (1) and are given by $W_i = (1 + k_i^2\hat{\rho}^2)|\phi_i|^2$. Thus, using the definitions of the equivalent quanta, Eqs. (25)–(28), the fractional energy changes for the modes can be obtained,

$$\frac{\Delta W_2}{\Delta W_1} = -\frac{(k_1^2 - k_3^2)(k_4^2 - k_1^2)}{(k_3^2 - k_2^2)(k_4^2 - k_2^2)}X_2, \tag{39}$$

$$\frac{\Delta W_3}{\Delta W_1} = -\frac{(k_1^2 - k_2^2)}{(k_3^2 - k_2^2)}X_3, \tag{40}$$

$$\frac{\Delta W_4}{\Delta W_1} = -\frac{(k_1^2 - k_2^2)}{(k_4^2 - k_2^2)}X_4. \tag{41}$$

Choosing a value for X_2 in the allowed range, X_3 and X_4 can be obtained from Eqs. (36) and (37) yielding the energy ratios transferred to the modes k_2, k_3, and k_4. The conservation of energy between the four interacting modes follows automatically from Eqs. (36), (37), and (39)–(41),

$$\frac{\Delta W_2}{\Delta W_1} + \frac{\Delta W_3}{\Delta W_1} + \frac{\Delta W_4}{\Delta W_1} + 1 = 0. \tag{42}$$

Similarly, obtaining the expression for the enstrophy of a mode from the CHM equation (cf. Ref. 3), $U_i = k_i^2 W_i$, the corresponding results for the fractional enstrophy changes are

$$\frac{\Delta U_2}{\Delta U_1} = -\frac{k_2^2(k_1^2 - k_3^2)(k_4^2 - k_1^2)}{k_1^2(k_3^2 - k_2^2)(k_4^2 - k_2^2)}X_2, \tag{43}$$

$$\frac{\Delta U_3}{\Delta U_1} = -\frac{k_3^2(k_1^2 - k_2^2)}{k_1^2(k_3^2 - k_2^2)}X_3, \tag{44}$$

$$\frac{\Delta U_4}{\Delta U_1} = -\frac{k_4^2(k_1^2 - k_2^2)}{k_1^2(k_4^2 - k_2^2)}X_4. \tag{45}$$

Using Eq. (36), (37), and (43)–(45) guarantee the conservation of wave enstrophy for the four-wave interaction.

$$\frac{\Delta U_2}{\Delta U_1} + \frac{\Delta U_3}{\Delta U_1} + \frac{\Delta U_4}{\Delta U_1} + 1 = 0. \tag{46}$$

It is also worth noting that the fractional changes in the equivalent quanta X_2, X_3, and X_4, unlike the corresponding three-wave quantities (cf. Ref. 8), are no longer constrained to integer values.

IV. THE GENERALIZED CHARNEY-HASEGAWA-MIMA EQUATION

The case when the lowest frequency mode $(\omega_2, \mathbf{k}_2)$ is a zonal flow, for which $k_{2y} = 0$, and hence $\omega_2 = 0$ is of particular interest due to its influence on transport reduction as shown in Ref. 4. As pointed out in Ref. 3, this case requires special treatment. By allowing for the presence of a zonal flow at the outset, the nonlinear behavior of the electrostatic potential is described by the generalized Charney-Hasegawa-Mima equation:

$$\left(\frac{\partial}{\partial t} + \mathbf{V}_0 \cdot \nabla + \mathbf{V}_d \cdot \nabla\right)\frac{e\widetilde{\phi}}{T_e}$$

$$- \left(\frac{\partial}{\partial t} + \mathbf{V}_0 \cdot \nabla + \widetilde{\mathbf{V}}_E \cdot \nabla\right)\rho_s^2 \nabla_\perp^2 \frac{e\phi}{T_e} = 0. \tag{47}$$

Here ϕ is the total electrostatic potential given by $\phi = \bar{\phi} + \widetilde{\phi}$, where $\bar{\phi}$ is the y-averaged part and $\widetilde{\phi}$ represents the fluctuation. The velocity $\mathbf{V}_0 = c\hat{\mathbf{z}} \times \nabla \bar{\phi}/B$ is the y-averaged part of

the $\mathbf{E} \times \mathbf{B}$ drift and is referred to as the zonal flow, where the equilibrium magnetic field is $\mathbf{B} = B\hat{\mathbf{z}}$. $\mathbf{V}_d = V_d\hat{\mathbf{y}}$ is the diamagnetic drift with $V_d = c_s^2/(\Omega_i L_n)$, and L_n is the equilibrium density scale length, $L_n^{-1} = 1/\bar{n}|d\bar{n}/dx|$, while $\widetilde{\mathbf{V}}_E = c\hat{\mathbf{z}} \times \nabla\widetilde{\phi}/B$ is the fluctuating $\mathbf{E} \times \mathbf{B}$ drift and $\rho_s = c_s/\Omega_i$. Following Ref. 10, the system dimensions in the x and y directions are taken as a, and the standard normalizations [cf. Eq. (1)] are used: $\hat{\rho} = \rho_s/a$, $\phi \to e\phi/T_e$, $x \to x/a$, $y \to y/a, t \to (\rho_s c_s/a^2)t$, $\mathbf{V}_{\mathbf{E} \times \mathbf{B}} = (\rho_s c_s/a)\hat{\mathbf{z}} \times \nabla\phi$, and $V_d = \alpha\rho_s c_s/a$, where $\alpha = a/L_n$. With these normalizations, Eq. (47) can be cast into a pair of dimensionless nonlinear, coupled equations for $\bar{\phi}(x,t)$ and $\hat{f} \equiv (1 - \hat{\rho}^2\nabla_\perp^2)\widetilde{\phi}$,

$$\frac{\partial\bar{\phi}_{xx}}{\partial t} + \langle\hat{\Sigma}(x,y)\rangle_y = 0, \tag{48}$$

$$\frac{\partial\hat{f}}{\partial t} + \nabla \cdot (\mathbf{V}_0\hat{f}) - \hat{\rho}^2[\hat{\Sigma}(x,y) - \langle\hat{\Sigma}(x,y)\rangle_y] + \alpha\frac{\partial\widetilde{\phi}}{\partial y}$$

$$+ \hat{\rho}^2\frac{\partial\widetilde{\phi}}{\partial y}\frac{\partial\bar{\phi}_{xx}}{\partial x} = 0, \tag{49}$$

where $\hat{\Sigma}(x,y) = (\mathbf{z} \times \nabla\widetilde{\phi}) \cdot \nabla\nabla_\perp^2\widetilde{\phi}$. The equations describing a four-wave interaction, in which one of the modes is a zero-frequency zonal flow, can be obtained from Eq. (47) or Eqs. (48) and (49). The equations have already been derived in Ref. 11 and are as follows:

$$\frac{dA_0}{dt} = -\Omega_0\frac{[1 + (k_+^2 - q^2)\hat{\rho}^2]}{(1 + k_0^2\hat{\rho}^2)}a_+B^*$$

$$+ \Omega_0\frac{[1 + (k_-^2 - q^2)\hat{\rho}^2]}{(1 + k_0^2\hat{\rho}^2)}a_-B, \tag{50}$$

where A_0 is the pump wave, $a_\pm$ the sideband drift waves, and B the zonal flow. The wave numbers are normalized to a, the system size, the pump wave number is $\mathbf{k}_0 = (k_x, k_y, 0)$, the zonal flow wave number is $\mathbf{q} = (q, 0, 0)$, and the sideband wave numbers are $\mathbf{k}_\pm = (k_x \pm q, k_y, 0)$. The quantity $\Omega_0 = qk_y$. The equations satisfied by $a_\pm, B$ are

$$\frac{da_+}{dt} + i\delta_+a_+ = \Omega_0\frac{[1 + (k_0^2 - q^2)\hat{\rho}^2]}{(1 + k_+^2\hat{\rho}^2)}A_0B, \tag{51}$$

$$\frac{da_-}{dt} + i\delta_-a_- = -\Omega_0\frac{[1 + (k_0^2 - q^2)\hat{\rho}^2]}{(1 + k_-^2\hat{\rho}^2)}A_0B^*, \tag{52}$$

$$\frac{dB}{dt} = \Omega_0\frac{(k_+^2 - k_0^2)}{q^2}a_+A_0^* - \Omega_0\frac{(k_-^2 - k_0^2)}{q^2}a_-^*A_0, \tag{53}$$

where $\delta_\pm = \omega_\pm - \omega_0$, $k_0^2 = k_x^2 + k_y^2$, $k_\pm^2 = (k_x \pm q)^2 + k_y^2$, $\omega_0 = \alpha k_y/(1 + k_0^2\hat{\rho}^2)$, and $\omega_\pm = \alpha k_y/(1 + k_\pm^2\hat{\rho}^2)$.

Initially, when $|A_0| \gg |a_\pm|$ and $|B|$, Eqs. (51)–(53) give rise to a modulational instability described in Refs. 10 and 11. The threshold for the instability is given by (in dimensional variables)

$$|A_0|^2 > (\rho_s q)^2 \frac{V_d^2}{2c_s^2}, \tag{54}$$

with an unstable band of wave numbers given by

$$0 < \rho_s q < \sqrt{2} \frac{c_s}{V_d} |A_0|. \tag{55}$$

The wave number for maximum growth is given by

$$(\rho_s q)_{max} = \frac{c_s}{V_d} |A_0|. \tag{56}$$

Similar to the general four-wave case described in Sec. III, we again derive conservation relations for the four-wave interactions with a zonal flow. Proceeding as in Sec. III, the equations for the intensities are

$$\frac{d}{dt}|A_0|^2 = -\Omega_0 \frac{[1 + (k_+^2 - q^2)\hat{\rho}^2]}{(1 + k_0^2 \hat{\rho}^2)} a_+ B^* A_0^*$$
$$+ \Omega_0 \frac{[1 + (k_-^2 - q^2)\hat{\rho}^2]}{(1 + k_0^2 \hat{\rho}^2)} a_- B A_0^* + \text{c.c.}, \tag{57}$$

$$\frac{d}{dt}|a_+|^2 = \Omega_0 \frac{[1 + (k_0^2 - q^2)\hat{\rho}^2]}{(1 + k_+^2 \hat{\rho}^2)} a_+^* A_0 B + \text{c.c.}, \tag{58}$$

$$\frac{d}{dt}|a_-|^2 = -\Omega_0 \frac{[1 + (k_0^2 - q^2)\hat{\rho}^2]}{(1 + k_-^2 \hat{\rho}^2)} a_-^* A_0 B^* + \text{c.c.}, \tag{59}$$

$$\frac{d}{dt}|B|^2 = \Omega_0 \frac{(k_+^2 - k_0^2)}{q^2} B^* a_+ A_0^* - \Omega_0 \frac{(k_-^2 - k_0^2)}{q^2} B a_- A_0 + \text{c.c.} \tag{60}$$

Introducing the equivalent quanta of the modes,

$$N_0 = [1 + (k_0^2 - q^2)\hat{\rho}^2](1 + k_0^2 \hat{\rho}^2)|A_0|^2, \tag{61}$$

$$N_+ = [1 + (k_+^2 - q^2)\hat{\rho}^2](1 + k_+^2 \hat{\rho}^2)|a_+|^2, \tag{62}$$

$$N_- = [1 + (k_-^2 - q^2)\hat{\rho}^2](1 + k_-^2 \hat{\rho}^2)|a_-|^2, \tag{63}$$

it is straight forward to obtain the following conservation relation from Eqs. (57)–(59):

$$\frac{d}{dt}(N_0 + N_+ + N_-) = 0. \tag{64}$$

A second conservation relation is obtained from Eqs. (58)–(60),

$$\frac{d}{dt}\left\{ q^2|B|^2 - \frac{(k_+^2 - k_0^2)}{[1 + (k_0^2 - q^2)\hat{\rho}^2][1 + (k_+^2 - q^2)\hat{\rho}^2]} N_+ \right.$$
$$\left. - \frac{(k_-^2 - k_0^2)}{[1 + (k_0^2 - q^2)\hat{\rho}^2][1 + (k_-^2 - q^2)\hat{\rho}^2]} N_- \right\} = 0. \tag{65}$$

Just as in the previous case, the quantities N_0, $N_\pm$, and $q^2|B|^2$ control the distribution of energy and enstrophy between the sidebands and the associated zonal flows. To demonstrate this, consider the incremental changes ΔN_0, ΔN_+, and ΔN_- to N_0, N_+, and N_-, and $\Delta|B|^2$ to $|B|^2$. The conservation relations then become

$$\Delta N_0 + \Delta N_+ + \Delta N_- = 0, \tag{66}$$

$$q^2 \Delta|B|^2 - \frac{(k_+^2 - k_0^2)}{[1 + (k_0^2 - q^2)\hat{\rho}^2][1 + (k_+^2 - q^2)\hat{\rho}^2]} \Delta N_+$$
$$- \frac{(k_-^2 - k_0^2)}{[1 + (k_0^2 - q^2)\hat{\rho}^2][1 + (k_-^2 - q^2)\hat{\rho}^2]} \Delta N_- = 0. \tag{67}$$

Defining

$$-\frac{\Delta N_+}{\Delta N_0} = X_+, \tag{68}$$

$$-\frac{\Delta N_-}{\Delta N_0} = X_-, \tag{69}$$

Eq. (66) becomes

$$X_+ + X_- = 1. \tag{70}$$

Similarly, defining

$$-\hat{\rho}^2 q^2 \frac{\Delta|B|^2}{\Delta N_0} = Y, \tag{71}$$

with $\alpha_\pm = 1 + (k_\pm^2 - q^2)\hat{\rho}^2$ and $\alpha_0 = 1 + (k_0^2 - q^2)\hat{\rho}^2$, Eq. (67) becomes

$$Y = \frac{1}{\alpha_0} - \left(\frac{X_+}{\alpha_+} + \frac{X_-}{\alpha_-} \right), \tag{72}$$

where we have made use of Eq. (70). As for the general four-wave case described in Sec. III there are again three unknowns but only two equations. Since $0 < X_+ < 1$, Eq. (72) constrains the range of values of Y. Choosing a value of Y in this range allows $X_\pm$ to be determined.

The energies of the pump wave, sidebands, and zonal flow are defined by the exact invariants (cf. Ref. 11) of the generalized CHME and are

$$W_0 = (1 + k_0^2 \hat{\rho}^2)|A_0|^2, \tag{73}$$

$$W_\pm = (1 + k_\pm^2 \hat{\rho}^2)|a_\pm|^2, \tag{74}$$

$$W_B = \hat{\rho}^2 q^2 |B|^2. \tag{75}$$

Expressing the ratios $\Delta W_\pm / \Delta W_0$ and $\Delta W_B / \Delta W_0$ in terms of $X_\pm$ and Y, we obtain the following relations:

$$\frac{\Delta W_+}{\Delta W_0} = -\frac{\alpha_0}{\alpha_+} X_+, \tag{76}$$

$$\frac{\Delta W_-}{\Delta W_0} = -\frac{\alpha_0}{\alpha_-} X_-, \tag{77}$$

$$\frac{\Delta W_B}{\Delta W_0} = -\alpha_0 Y. \tag{78}$$

With the aid of Eq. (72), Eqs. (76)–(78) guarantee the conservation of energy for the four-wave interaction,

$$\frac{\Delta W_B}{\Delta W_0} + \frac{\Delta W_+}{\Delta W_0} + \frac{\Delta W_-}{\Delta W_0} + 1 = 0. \tag{79}$$

Similarly, the enstrophies of the individual modes are defined by the exact invariants derived in Ref. 11 and are as follows:

$$U_0 = (1 + k_0^2 \hat{\rho}^2)^2 |A_0|^2, \tag{80}$$

$$U_\pm = (1 + k_\pm^2 \hat{\rho}^2)^2 |a_\pm|^2, \tag{81}$$

$$U_B = \hat{\rho}^4 q^4 |B|^2. \tag{82}$$

The incremental enstrophy ratios are given in terms of $X_\pm$ and Y by

$$\frac{\Delta U_+}{\Delta U_0} = -\frac{(1 + k_+^2 \hat{\rho}^2)\alpha_0}{(1 + k_0^2 \hat{\rho}^2)\alpha_+} X_+, \tag{83}$$

$$\frac{\Delta U_-}{\Delta U_0} = -\frac{(1 + k_-^2 \hat{\rho}^2)\alpha_0}{(1 + k_0^2 \hat{\rho}^2)\alpha_-} X_-, \tag{84}$$

$$\frac{\Delta U_B}{\Delta U_0} = -\frac{\hat{\rho}^2 q^2 \alpha_0}{(1 + k_0^2 \hat{\rho}^2)} Y. \tag{85}$$

Again, using Eq. (72), Eqs. (83)–(85) lead to the conservation of enstrophy for the four-wave interaction,

$$\frac{\Delta U_B}{\Delta U_0} + \frac{\Delta U_+}{\Delta U_0} + \frac{\Delta U_-}{\Delta U_0} + 1 = 0. \tag{86}$$

For a given pump wave, there is a spectrum of unstable zonal flows with wave numbers q and their associated sidebands. The relations given in Eqs. (76)–(78) and (83)–(85) determine the rates at which energy and enstrophy are transferred to this system of modes in the initial stages of their evolution.

V. NUMERICAL SIMULATION OF THE GENERALIZED CHARNEY-HASEGAWA-MIMA EQUATION

In this section a full account is given of the results of numerical simulation of the GCHME as described by Eqs. (48) and (49). A summary of these results was given in Ref. 10.

A system consisting of a finite-amplitude drift wave coupled through a zonal flow fluctuation to sidebands is unstable to a modulational instability as discussed in the previous section and at length in Ref. 11. A question of fundamental interest is how such an instability evolves towards a fully nonlinearly saturated state when the initial conditions are such that many modulationally unstable and stable modes exist to start with. It might be naively expected that the fastest growing modes would dominate. This leads to the further questions: Will this dominance persist and what, if any, are the roles of the other modes, both unstable and stable? These questions are answered by the numerical simulation.

For these simulations, the pump-wave number is given by $\mathbf{k} = 2\pi(m_x, m_y, 0)$, where m_x and m_y are integers, remembering that the wave number is normalized to the inverse of the system size a. Similarly, the zonal flow wave number is $\mathbf{q} = 2\pi(m_q, 0, 0)$, where m_q is also an integer. It should be
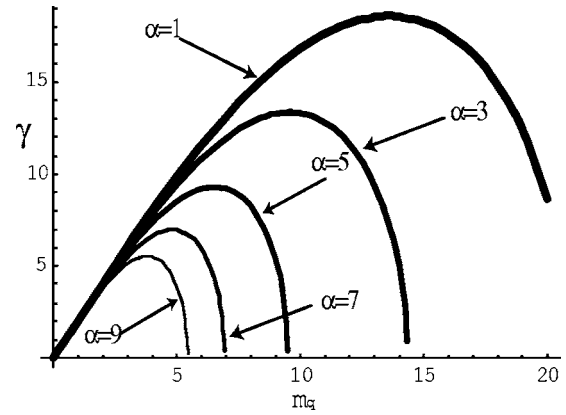

FIG. 1. The dispersion relation for the modulational instability. The growth rate is plotted as a function of the zonal flow mode number for several values of α.

noted that although the initial state consists of just the pump wave and its sidebands the simulations themselves are general and allow for the evolution of all modes, within the allowed numerical scales of resolution.

The parameters of the numerical simulations are $\alpha = 3$, $\hat{\rho} = 7.5 \times 10^{-3}$, $m_x = m_y = 4$, and $A_0 = 0.01$. For these parameters, the band of unstable wave numbers given by Eq. (55) is illustrated in Fig. 1 (taken from Fig. (7) of Ref. 11) and shows that the unstable band runs from $m_q = 1$ to $m_q = 14$ with the fastest-growing modes occurring for $m_q = 9$ and 10. We emphasize the fact that our initial conditions in this case consisted of some stable modes as well, since we considered modes up to and including $m_q = 16$.

The initial state of the simulation is taken to be one in which all the unstable sidebands ($m_x \pm m_q$ and m_y) are present at the same low amplitude (10^{-6} of the pump amplitude). The results of the simulation are shown in Figs. 2 and 3.

Figure 2(a) shows the surface plots of the Fourier amplitudes $\tilde{\phi}$ as functions of m_x (for $m_x \geq 0$) and time, while Fig. 2(b) illustrates the corresponding Fourier amplitudes of the zonal flow potential $\bar{\phi}$ as functions of m_q and time. The pump wave corresponds to $m_x = 4$. Negative values of m_x are not shown, as the spectrum is symmetric about $m_x = 4$. Initially, the fastest-growing modes can be seen to dominate, fulfilling naive expectations based on linear growth. These are the modes, shown in Fig. 2(a), which are clustered around $m_x = 13, 14$, namely, $m_x + m_q$, with $m_x = 4$, corresponding to the pump and $m_q = 9$ and 10 corresponding to the fastest-growing modulationally unstable modes. Similarly, Fig. 2(b) shows the zonal flow modes dominated by the fastest-growing modes, $m_q = 9$ and 10 initially.

However, an additional feature, which was not anticipated, is clearly illustrated in both Figs. 2(a) and 2(b). This is the appearance of much faster growing, long-wavelength modes, occurring at $m_x = 5$ and $m_q = 1$. These modes, initially slowly growing, eventually overtake the shorter wavelength modes in the later stages of the simulation. This behavior is also illustrated in Figs. 3(a) and 3(b), which compare the time dependence of the pump wave and upper sidebands associated with $m_q = 10$ and $m_q = 1$ and the zonal flows related to these mode numbers, respectively. Figure 3(a) shows the
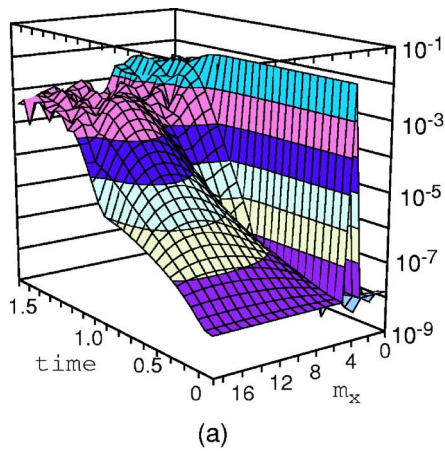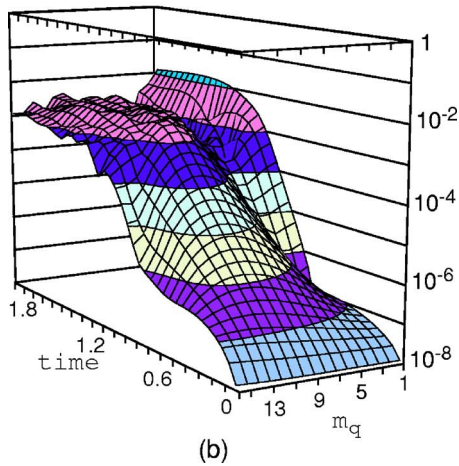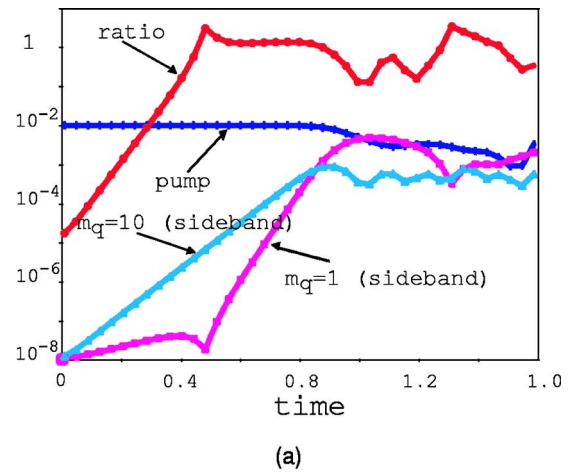
FIG. 2. Surface plots of the Fourier amplitudes of (a) $\tilde{\phi}$ and (b) $\bar{\phi}$ as a function of time and m_x and m_q, respectively.

FIG. 3. Time evolution of (a) the pump amplitude and upper sidebands with $m_q=1$ and 10, and (b) zonal flow amplitudes for $m_q=1$ and 10.
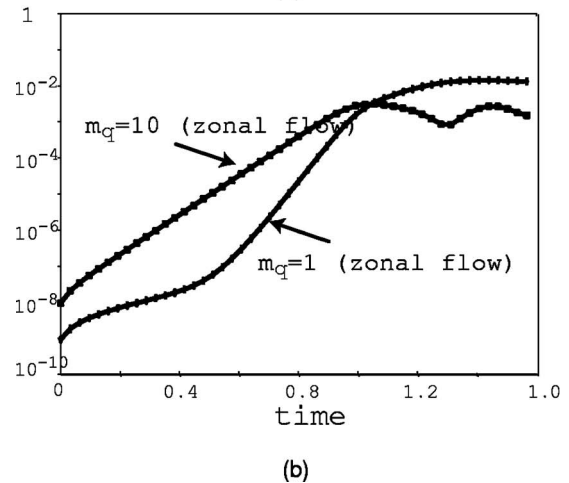
upper sideband amplitude associated with $m_q=10$ (one of the fastest-growing modes, cf. Fig. 1) and the upper sideband amplitude associated with $m_q=1$ (one of the slowest of the modulationally unstable modes). The $m_q=10$ upper sideband can be seen to grow at its modulationally unstable rate until the pump wave begins to deplete at about $t=1$. In complete contrast, the $m_q=1$ upper sideband grows at its modulational rate initially but then undergoes an abrupt transition at $t=0.5$, after which it grows at a faster rate than the $m_q=10$ mode which it overtakes at $t=0.9$. It is clear from the time dependence of the pump wave, also shown in Fig. 3(a), that the long-wavelength sideband overtakes the short-wavelength mode before pump depletion occurs. The significance of the curve labeled "ratio" will be discussed in the next section where an interpretation of these results is given. The zonal flow amplitudes of the short-wavelength, fast-growing, $m_q=10$ mode and the long-wavelength $m_q=1$ mode are plotted in Fig. 3(b). The short- and long-wavelength modes exhibit a similar time dependence to the sideband modes.

VI. A BEAT MECHANISM FOR RAPID SPECTRAL TRANSFER

A striking feature of the results of the numerical simulation shown in the previous section is the evolution of the

long-wavelength zonal flow and its associated sidebands to an enhanced growth, exceeding the rate of the fastest-growing modulationally unstable modes. In fact, from the numerical simulation, the enhanced growth rate was found to be $2\gamma_{\max}$.

The analysis leading to the modulational instability will now be modified by means of an additional feature suggested by the results of the numerical simulation. Instead of considering a representative zonal flow wave number, two zonal flow wave numbers q and p are introduced, and it will be assumed, without loss of generality, that $q>p>0$. In the numerical simulations, $q=2\pi m_q$ and $p=2\pi m_p$, with $m_q>m_p$. Both q and p will be assumed to be in the band of modulationally unstable wave numbers, and furthermore, they will be taken to be at or close to the fastest-growing mode. The zonal flow with wave number q is associated with sidebands ($k_x\pm q$, k_y, and 0) which grow at the rate γ_q given by Eq. (47) in Ref. 11. This zonal flow amplitude will be denoted by B_{m_q} and its sidebands by $a_{k_x\pm q,k_y}\equiv a_{\pm m_q}$. Similarly, the zonal flow with wave number p and its sidebands grow at the rate γ_p given by the same modulational instability dispersion relation, and are denoted by B_{m_p} and $a_{\pm m_p}$, respectively.

It is clear that the fastest-growing, modulationally unstable modes will dominate the system evolution initially.

However, the longest-wavelength zonal flow mode, which is driven by $A_0^* a_1$ and $A_0 a_{-1}^*$, is also driven by the beating of two of the fastest-growing modes through the terms $a_{m_q} a_{m_p}^*$ and $a_{-m_q}^* a_{-m_p}$ to produce the difference wave number $q-p$. Both of these terms grow at the sum of the growth rates $\gamma_q + \gamma_p$. Similar arguments apply to the sidebands $a_{\pm 1}$ associated with the longest wavelength zonal flow. The long-wavelength sidebands are initially driven by $A_0 B_{\pm 1}$, where $B_{-1} \equiv B_1^*$, but they are also driven by the zonal flows B_{m_q, m_p} and the sidebands $a_{\pm m_q}$ and $a_{\pm m_p}$. Although the pump wave is initially much larger than all the other modes, $A_0^* a_1$ and $A_0 a_{-1}^*$ will grow very slowly compared with the products $a_{m_q} a_{m_p}^*$ and $a_{-m_q}^* a_{-m_p}$. The latter terms can eventually overtake the pump driving terms. This qualitative discussion is now translated into a modification of the differential equations for the modulationally unstable modes given by Eqs. (50)–(53).

To facilitate the analysis, we introduce the difference and sum wave numbers, $\tau = q - p$ and $\sigma = q + p$, and the associated triads $(B_{m_\tau}, a_{m_\tau}, a_{-m_\tau})$ and $(B_{m_\sigma}, a_{m_\sigma}, a_{-m_\sigma})$. The modified equations follow from Eq. (47) or Eqs. (48) and (49) in a manner similar to the derivation of Eqs. (38)–(40) in Ref. 11. These modified equations have already been given in Ref. 10 and are, for the long-wavelength triad $(B_{m_\tau}, a_{m_\tau}, a_{-m_\tau})$,

$$\frac{dB_{m_\tau}}{dt} - \tau k_y \frac{(k_\tau^2 - k_0^2)}{\tau^2} a_{m_\tau} A_0^* + \tau k_y \frac{(k_{-\tau}^2 - k_0^2)}{\tau^2} a_{-m_\tau}^* A_0$$

$$= \tau k_y \frac{(k_q^2 - k_p^2)}{\tau^2} a_{m_q} a_{m_p}^* + \tau k_y \frac{(k_{-p}^2 - k_{-q}^2)}{\tau^2} a_{-m_p} a_{-m_q}^*, \quad (87)$$

$$\frac{da_{m_\tau}}{dt} + i\delta_\tau a_{m_\tau} - \tau k_y \frac{[1 + (k_0^2 - \tau^2)\hat\rho^2]}{(1 + k_\tau^2 \hat\rho^2)} A_0 B_{m_\tau}$$

$$= -p k_y \frac{[1 + (k_q^2 - p^2)\hat\rho^2]}{(1 + k_\tau^2 \hat\rho^2)} a_{m_q} B_{-m_p}$$

$$+ q k_y \frac{[1 + (k_{-p}^2 - q^2)\hat\rho^2]}{(1 + k_\tau^2 \hat\rho^2)} a_{-m_p} B_{m_q}, \quad (88)$$

$$\frac{da_{-m_\tau}}{dt} + i\delta_{-\tau} a_{-m_\tau} + \tau k_y \frac{[1 + (k_0^2 - \tau^2)\hat\rho^2]}{(1 + k_{-\tau}^2 \hat\rho^2)} A_0 B_{-m_\tau}$$

$$= p k_y \frac{[1 + (k_{-q}^2 - p^2)\hat\rho^2]}{(1 + k_{-\tau}^2 \hat\rho^2)} a_{-m_q} B_{m_p}$$

$$- q k_y \frac{[1 + (k_p^2 - q^2)\hat\rho^2]}{(1 + k_{-\tau}^2 \hat\rho^2)} a_{m_p} B_{-m_q}, \quad (89)$$

where $\delta_{\pm\tau} \equiv \omega_{\pm\tau} - \omega_0$, $\omega_{\pm\tau} = \alpha k_y / (1 + k_{\pm\tau}^2 \hat\rho^2)$, and $k_{\pm\tau}^2 = (k_x \pm \tau)^2 + k_y^2$. We have by the same token, $k_{\pm q}^2 = (k_x \pm q)^2 + k_y^2$, and $k_{\pm p}^2 = (k_x \pm p)^2 + k_y^2$. It should be apparent that Eq. (89) follows from Eq. (88) by merely changing $q \to -q$, $p \to -p$, and $\tau \to -\tau$. Note that $B_{m_q} = B_{-m_q}^*$. It follows that the homogeneous part of Eqs. (87)–(89) is identical with Eqs. (51)–(53) when the wave number q of the latter equations is identified with τ. Hence, the complementary solution of Eqs. (87)–(89) can be obtained by taking advantage of the different time scales between the modulationally fastest-growing modes and the

most slowly growing modes. The terms on the right-hand sides of Eqs. (87)–(89) are therefore treated as driving terms whose time dependence is given by the solutions of the homogeneous equations for the fastest-growing, modulationally unstable triads $(B_{m_q}, a_{m_q}, a_{-m_q})$ and $(B_{m_p}, a_{m_p}, a_{-m_p})$. Clearly, all the driving terms will then have the same time dependence given by $\exp[i(\Omega_q - \Omega_p)t + (\gamma_q + \gamma_p)t]$, where Ω_q and Ω_p are the real parts of the solution of the modulational instability dispersion relation [i.e., Eq. (47) in Ref. 11]. The particular integrals of Eqs. (87)–(89) will therefore be proportional to $\exp(\gamma_q + \gamma_p)t$, growing at a rate very close to twice the maximum growth rate of the original modulational instability. The q and p triads will play a significant role in the time evolution once the products such as $a_{m_q} a_{m_p}^*$ have grown to the level of, say, $a_{m_\tau} A_0^*$. This important point is illustrated quantitatively in Fig. 3(a) where the ratio $(k_q^2 - k_p^2) a_{m_q} a_{m_p}^* / (k_\tau^2 - k_0^2) a_{m_\tau} A_0^*$ is plotted as a function of time. The ratio increases from its initially very small value until it reaches the value 1 at a time $t = 0.5$ which is precisely the time at which the abrupt transition occurs in the growth of the $m_q = 1$ upper sideband. It should also be noted that pump depletion does not begin until well after this time, thus validating the assumption made in the approximate solution of Eqs. (87)–(89). The transition in the growth of the $m_q = 1$ zonal flow also occurs at the same critical time.

It is interesting to note that the ratio, having reached the value of 1, hovers around this value until pump depletion begins. This is evidently due to the fact that once the long-wavelength modes change to their enhanced growth rate, both terms in the ratio will then grow at $2\gamma_{max}$. As a final confirmation of this interpretation, a linear fit of the data gives the growth rates of the three fastest-growing modes as $\gamma_9 = 13.4$, $\gamma_{10} = 13.6$, and $\gamma_{11} = 13.4$ while the nonlinear rate of the $m_q = 1$ sideband is $\gamma_1 = 26.6$ which is very close to the sum of the growth rates of the two fastest-growing modes.

The nonlinear beat mechanism just described, which leads to the enhancement in the growth of the $m_q - m_p = 1$ zonal flow and its sidebands, will also operate on the other slowly growing modes, e.g., the $m_q - m_p = 2$ and 3 zonal flows and their associated sidebands. The longest-wavelength mode $m_q - m_p = 1$ is the most strongly driven one because the beating modes are closer together in wave-number space and more of them will contribute from the region of the fastest growth rate. This will be illustrated below with further results from the simulation.

It is also clear that the nonlinear beat excitation is not limited to the long-wavelength, modulationally unstable part of the spectrum of modes. The fast-growing modes that beat to drive the longest-wavelength difference mode can drive a short-wavelength sum mode triad $(B_{m_\sigma}, a_{m_\sigma}, a_{-m_\sigma})$, where $\sigma = q + p$. These short-wavelength modes lie in the modulationally stable region of the wave-number spectrum, but will be driven with the same growth rate $\gamma_q + \gamma_p$ as is the enhanced long-wavelength difference mode. In the short-wavelength case the drive oscillates at the frequency $\Omega_q + \Omega_p$. This case will also be illustrated with results from the simulation. The above discussion accounts for the main features of the surface plots given in Figs. 2(a) and 2(b) and the behavior il-
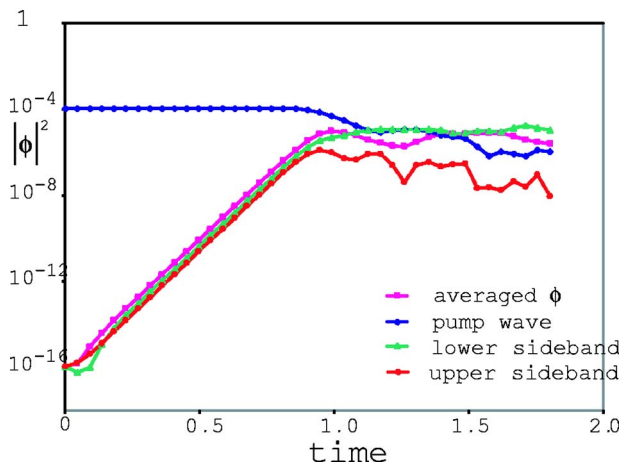
FIG. 4. Intensities of the pump wave ($|A_0|^2$), zonal flow ($|B|^2$), and associated sidebands ($|a_+|^2$ and $|a_-|^2$), for $m_q=10$.

FIG. 6. Intensities of the pump wave ($|A_0|^2$), zonal flow ($|B|^2$), and associated sidebands ($|a_+|^2$ and $|a_-|^2$), for $m_q=13$.

lustrated in Figs. 3(a) and 3(b). In the next section, the dynamics of the modes is shown in more detail. In particular, it will be shown how the modes separate into two categories in terms of their evolution.

VII. TIME EVOLUTION OF THE MODES

For the parameters of the numerical simulation given in Sec. V, the band of modulationally unstable wave numbers range from $m_q=1$ to $m_q=14$. Referring again to Fig. 1, the fastest-growing modes can be seen to lie in the range from $m_q=5$ to $m_q=13$. The evolution of the fastest-growing modulationally unstable modes will now be compared with that of the weakly modulationally unstable long-wavelength modes and with the short-wavelength, modulationally stable modes.

A selection of the fastest-growing modes is shown in Figs. 4–6. The $m_q=10$ zonal flow and associated upper and lower sideband intensities are plotted in Fig. 4 as functions of time with the pump-wave intensity shown for reference. The zonal flow and sidebands (the modes corresponding to the maximum growth rate for the modulational instability) all grow at the same rate, in agreement with the analytic theory, presented in Sec. VI. The modes grow until the pump
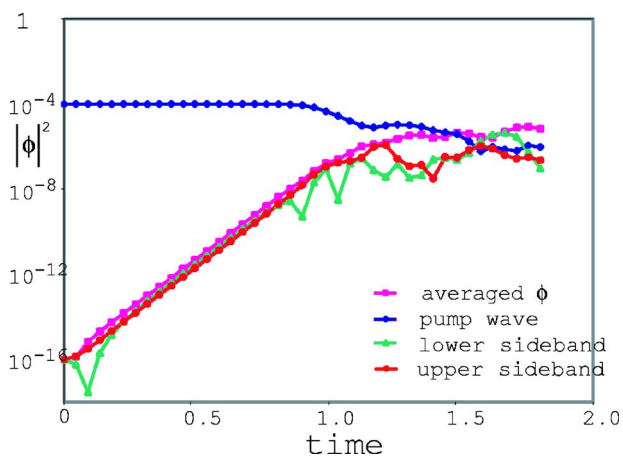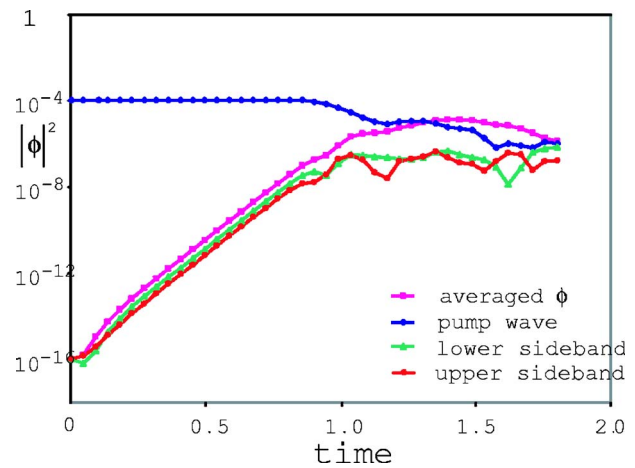
begins to deplete at $t \simeq 1$. Figures 5 and 6 show a similar behavior for the intensities of the $m_q=6$ and $m_q=13$ zonal flows and associated sidebands, respectively.

The evolution of the weakly (modulationally) unstable long-wavelength modes is illustrated in Figs. 7–9. Figure 7 shows the longest-wavelength zonal flow $m_q=1$ and its sidebands, again with the pump for comparison. The slow initial growth is more influenced by transients for the three modes but at the critical time when the transition to the enhanced growth occurs, all the three modes grow at close to twice the maximum growth rate. Although the intensity of the $m_q=1$ zonal flow significantly exceeds the pump intensity, its energy is much less. The corresponding evolution of the $m_q=2$ and $m_q=3$ zonal flows and associated sidebands is shown in Figs. 8 and 9. A similar behavior of weak initial growth followed by an abrupt transition to an enhanced growth rate is also found. For $m_q=2$ and $m_q=3$, the transition occurs at a slightly later time (particularly for $m_q=3$) because the nonlinear driving term is not so strong due to the greater separation of the modes contributing to the drive in the wavenumber space.

FIG. 5. Intensities of the pump wave ($|A_0|^2$), zonal flow ($|B|^2$), and associated sidebands ($|a_+|^2$ and $|a_-|^2$), for $m_q=6$.
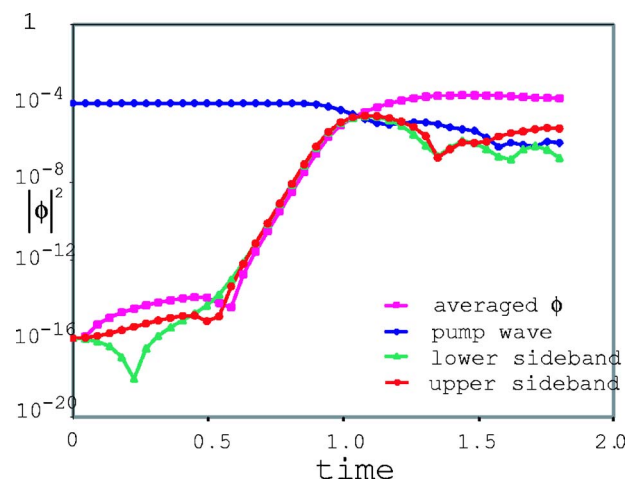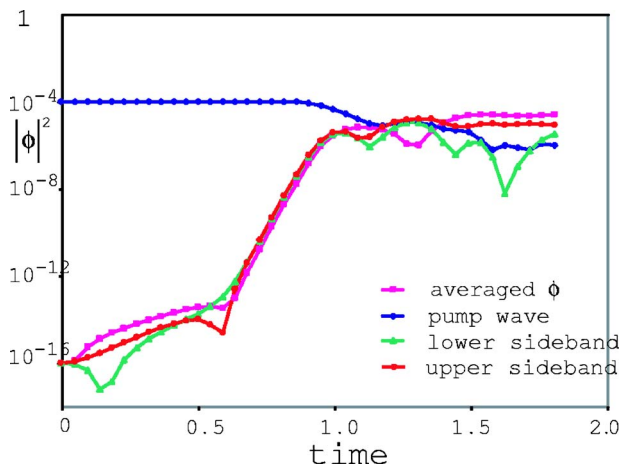

FIG. 7. Intensities of the pump wave ($|A_0|^2$), zonal flow ($|B|^2$), and associated sidebands ($|a_+|^2$ and $|a_-|^2$), for $m_q=1$.

FIG. 8. Intensities of the pump wave ($|A_0|^2$), zonal flow ($|B|^2$), and associated sidebands ($|a_+|^2$ and $|a_-|^2$), for $m_q=2$.

FIG. 10. Zonal flow intensities ($|\bar{\phi}|^2$) for the $m_q=1$, $m_q=10$, and $m_q=19$ modes.

The evolution of the short-wavelength, modulationally stable zonal flow $m_q=19$ is compared with the evolution of the $m_q=1$ and $m_q=10$ zonal flows. This is displayed in Fig. 10. The significance of these results is the following. The $m_q=10$ zonal flow is the fastest-growing, modulationally unstable mode whose time evolution has already been described. The $m_q=10$ mode can beat with a neighboring fast-growing mode ($m_q=9$), say, to generate the difference mode $m_q=1$ or the sum mode $m_q=19$.

Figure 10 shows that the evolution of the $m_q=1$, $m_q=10$, and $m_q=19$ zonal flows is quite distinct. As already discussed, the fast-growing $m_q=10$ mode grows at its modulational instability growth rate until pump depletion occurs. The long-wavelength, weakly modulationally unstable $m_q=1$ mode also grows at its modulational rate until it undergoes the transition to $2\gamma_{max}$ at about $t=0.6$. In contrast, the short-wavelength mode, which is modulationally stable, does not undergo a transition, but grows at the enhanced nonlinear growth rate throughout and joins smoothly on to the enhanced growth rate of the $m_q=1$ mode at its transition time. The evolution of the long and short wavelengths only di-
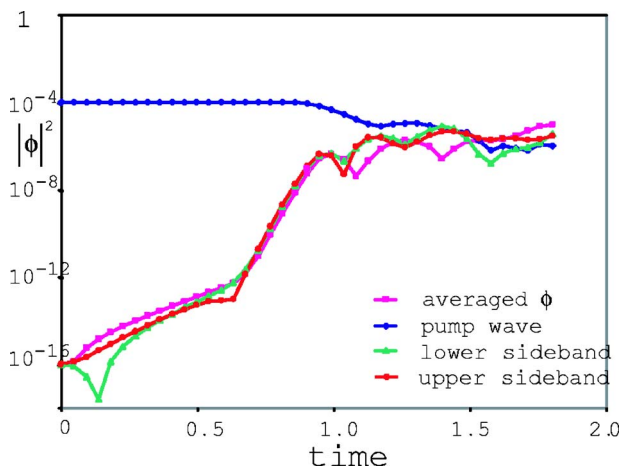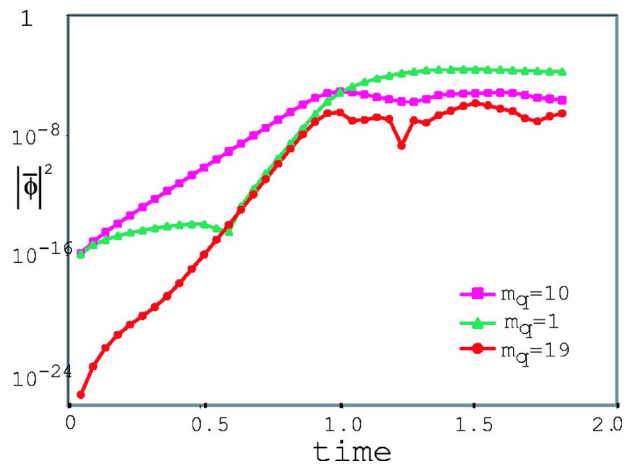
verges after pump depletion, when the system enters its fully nonlinear stage.

This section concludes with a brief description of the evolution of the energies and equivalent actions (equivalent quanta) of the modes. The incremental actions X_+, X_-, and Y were defined by Eqs. (68)–(71). These are normalized to the incremental change of action of the pump for a particular four-wave interaction with respect to a specific zonal flow mode number. Thus X_+, X_-, and Y refer to the upper sideband, lower sideband, and zonal flow, respectively. The dependence of the incremental actions on the time is illustrated in Fig. 11 for the case when $m_q=10$. The significant features of this figure are that after a brief period of transient behavior the incremental actions remain steady with values of 0.5 for the sidebands and $\simeq 0.25$ for the zonal flow; the sum $X_+ + X_- = 1$, as it should, but after a certain time, this four-wave sum rule is violated and the incremental actions are no longer steady. This latter phase is to be expected since the four-wave invariants are not exact invariants of the GCHME. Referring to Eqs. (76)–(78) which give the incremental energy changes for the modes, it is expected that for $m_q=10$, the energies of the zonal flow and sideband perturbations will be comparable. The two sidebands should gain approxi-
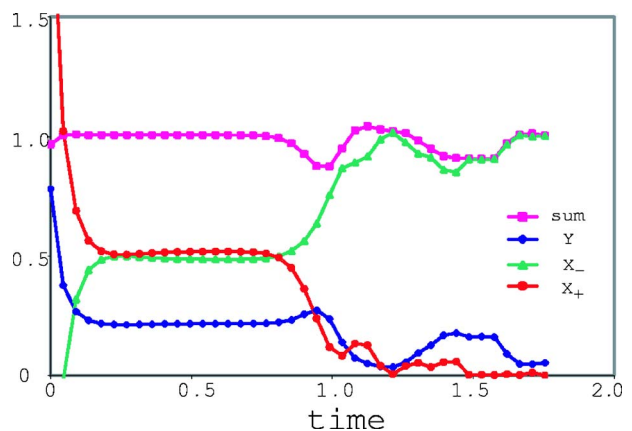

FIG. 9. Intensities of the pump wave ($|A_0|^2$), zonal flow ($|B|^2$), and associated sidebands ($|a_+|^2$ and $|a_-|^2$), for $m_q=3$.

FIG. 11. Time evolution of the incremental actions Y, X_+, and X_- for $m_q=10$.
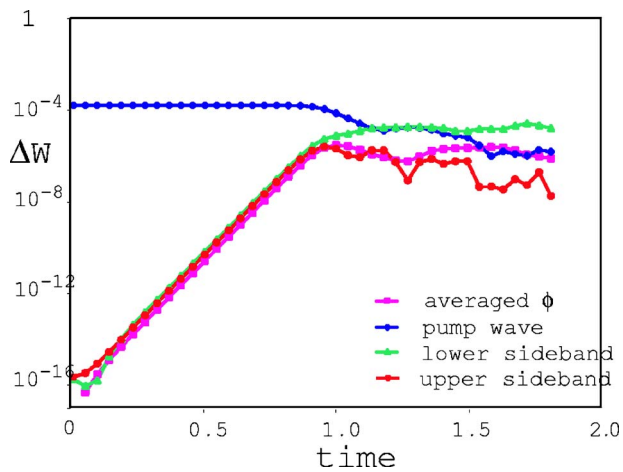
FIG. 12. Time evolution of the energy changes for the pump wave (ΔW_0), sidebands ($\Delta W_\pm$), and zonal flow (ΔW_B), for $m_q = 10$.

FIG. 14. Time evolution of the energy changes for the pump wave (ΔW_0), sidebands ($\Delta W_\pm$), and zonal flow (ΔW_B), for $m_q = 1$.

mately equal amounts of energy with the lower sideband gaining slightly more since $\alpha_+ > \alpha_-$. The change in the energies for the $m_q = 10$ zonal flow and its associated upper and lower sidebands is shown in Fig. 12 together with the energy of the pump. It can be seen that the energy changes are consistent with the predictions obtained above from the incremental actions.

A plot of the incremental actions as a function of time for the $m_q = 1$ zonal flow and its sidebands is shown in Fig. 13. This displays similar features to Fig. 10 except that the transient phase is more pronounced which is evidently due to the much slower initial growth of these modes. The sum rule $X_+ + X_- = 1$ holds for a significant period, even during the transient phase and $X_\pm$ remain steady at approximately 0.5 until the four-wave invariant is broken. In this case, the incremental action for the zonal flow is very small which implies that very little energy will be transferred to the zonal flow perturbation. This is borne out in Fig. 14 which shows the evolution of the energies of the modes corresponding to $m_q = 1$. It can be seen that the energy of the zonal flow, although increasing, is approximately three orders of magnitude less than the energies of the sidebands. The energies of the sidebands are almost exactly equipartitioned since X_- is
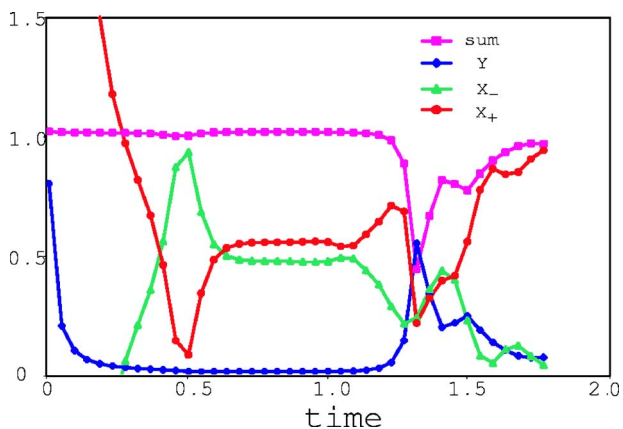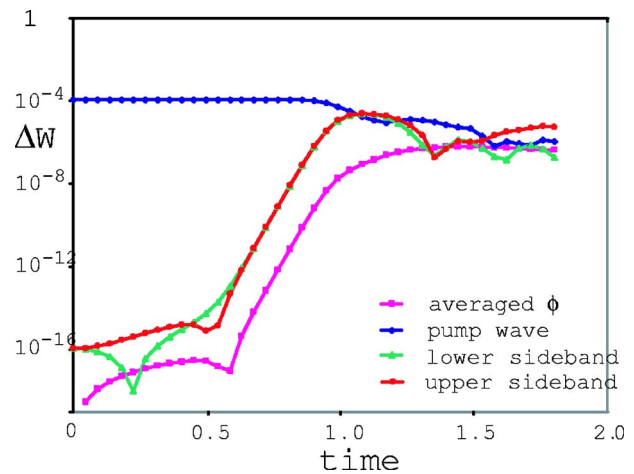
just below 0.5 and X_+ is just above 0.5, and $\alpha_+ > \alpha_-$. It is worth noting that for the case $m_q = 13$, $X_+ \simeq X_- \simeq Y \simeq 0.5$ and the energies transferred to the $m_q = 13$ zonal flow and its upper and lower sidebands are approximately equal.

The final result to be shown from the simulation is the resultant zonal flow which is made up of contributions of all the mode numbers. Although the $m_q = 1$ zonal flow potential is the largest in the saturated state, as shown in Fig. 3(b), the zonal flow is proportional to dB_q/dx. The resultant zonal flow as a function of x is illustrated in Fig. 15 and shows a fine structure (i.e., "corrugation") corresponding to $m_q = 10$ but with an asymmetry between positive and negative flows due to $m_q = 1$.

VIII. DISCUSSION AND CONCLUSIONS

This paper has been concerned with a study, both analytical and numerical, of the evolutionary dynamics towards a turbulent state of a finite-amplitude wave. A very simple fluid model has been employed in order to gain insight and understanding into the underlying mechanisms, with the ultimate aim of interpreting the results of both more realistic simulations (cf. Ref. 4) and experiments reported in Refs. 5 and 12. The fluid models used were the CHME and its generalization to allow for zonal flows, the GCHME.
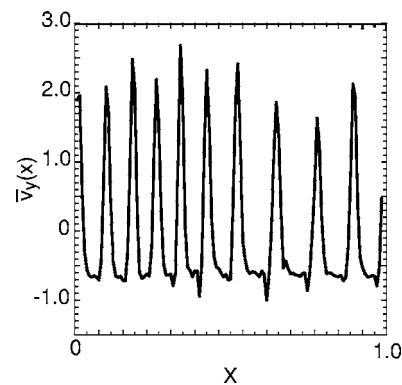

FIG. 13. Time evolution of the incremental actions $Y, X_+,$ and X_- for $m_q = 1$.

FIG. 15. Resultant zonal flow. Note the long wave envelope on sharp "jets."

The equivalent quanta, introduced in Ref. 8, have been generalized to the four-wave interaction for both the CHME and the GCHME. In both cases, it was shown that this approach leads automatically to the conservation of energy and enstrophy for the four-wave interactions. These four-wave invariants are specific to the reduced system and are not to be confused with the exact invariants of the full system derived in Ref. 11.

A numerical simulation of the GCHME has been described. The GCHME takes explicit account of zonal flows which are believed to be important in the dynamics of the formation and maintenance of transport barriers in confined plasmas and for similar regions of reduced transport in geophysical systems. The simulation presented shows the growth of the spectrum of modulationally unstable modes with the fastest-growing ones dominating the early development. However, it reveals an unexpected but clear secondary nonlinear mechanism which transforms the longest wavelength, weakly (modulationally) unstable modes into the most rapidly growing ones. This is shown to be important for the later evolution of the modes and is clearly a generic mechanism which should occur in many other turbulent systems where quadratic, conservative, advective nonlinearities in position space are important. A key feature of this mechanism is that it is a process which redirects the energy of the finite-amplitude pump wave, through the initially fastest-growing modes, to the slowest-growing modulationally unstable modes, and to short-wavelength, modulationally stable modes.

The integral invariants of this conservative system control the long-time saturation behavior of the turbulence. To investigate this is a challenging numerical task which is not attempted here although the code we have developed is capable in principle of studying the statistical distributions of energies (and enstrophies) in the modes modeled for long times. It should also be borne in mind that we do not include "profile-turbulence interactions" in the present paradigmatic model. In more realistic simulations allowance is made for the evolution of the density profile in the presence of turbulence. Such effects have been the subject of elaborate investigations including comparisons with experiments (see, for example, Refs. 13 and 14).

We wish to note here that the modulational instability and beating of strongly growing modes to generate sum and difference modes at the sum of the growth rates are very general mechanisms which must be implicated in all nonlinear systems with advective or Lorentz-force-type nonlinearities. Although we have discussed a very special conservative system in the GCHME, all spectral transfer processes in much more realistic systems (cf. Ref. 4) reveal very similar features to those reported here. In particular, the same mechanisms would also be expected to apply to the electron momentum channel in the presence of electromagnetic modes and sheared magnetic-field structures. The fact that long-wavelength parts of the spectra can be strongly driven by short-wavelength unstable modes can be expected to result in such phenomena as relaxation oscillations ("Elms" and "sawteeth") and in dynamo currents (analog of the zonal flows in the induction equation) which influence plasma self-organization as well as global transport scalings.

[1] J. C. Charney, J. Atmos. Sci. **28**, 1087 (1971).
[2] A. Hasegawa and K. Mima, Phys. Fluids **21**, 87 (1978).
[3] A. I. Smolyakov, P. H. Diamond, and V. I. Shevchenko, Phys. Plasmas **7**, 1349 (2000).
[4] A. Thyagaraja, P. J. Knight, and N. Loureiro, Eur. J. Mech. B/Fluids **23**, 475 (2004).
[5] K. H. Burrell, Science **281**, 1816 (1998).
[6] W. Horton and A. Hasegawa, Chaos **4**, 227 (1994).
[7] A. Smedman, U. Högström, and J. C. R. Hunt, Q. J. R. Meteorol. Soc. **130**, 31 (2004).
[8] A. Hasegawa and Y. Kodama, Phys. Rev. Lett. **41**, 1470 (1978).
[9] A. Hasegawa, C. G. McClennan, and Y. Kodama, Phys. Fluids **22**, 2122 (1979).
[10] D. R. McCarthy, C. N. Lashmore-Davies, and A. Thyagaraja, Phys. Rev. Lett. **93**, 065004 (2004).
[11] C. N. Lashmore-Davies, D. R. McCarthy, and A. Thyagaraja, Phys. Plasmas **8**, 5121 (2001).
[12] C. Gormezano, Plasma Phys. Controlled Fusion **41**, B367 (1999).
[13] M. R. de Baar, A. Thyagaraja, G. M. D. Hogeweij, P. J. Knight, and E. Min, Phys. Rev. Lett. **94**, 035002 (2005).
[14] A. Thyagaraja, P. J. Knight, M. R. de Baar, G. M. D. Hogeweij, and E. Min, Phys. Plasmas **12**, 090907 (2005).